Fe(II)-catalyzed transformation of Fe (oxyhydr)oxides across organic matter fractions in organically amended soils

Journal Pre-proof

Fe(II)-catalyzed transformation of Fe (oxyhydr)oxides across organic matter fractions in organically amended soils

Beatrice Giannetta, Ramona Balint, Daniel Said-Pullicino, César Plaza, Maria Martin, Claudio Zaccone

PII: S0048-9697(20)34654-4

DOI: https://doi.org/10.1016/j.scitotenv.2020.141125

Reference: STOTEN 141125

To appear in: *Science of the Total Environment*

Received date: 7 April 2020

Revised date: 17 July 2020

Accepted date: 18 July 2020

Please cite this article as: B. Giannetta, R. Balint, D. Said-Pullicino, et al., Fe(II)-catalyzed transformation of Fe (oxyhydr)oxides across organic matter fractions in organically amended soils, *Science of the Total Environment* (2020), https://doi.org/10.1016/j.scitotenv.2020.141125

Fe(II)-catalyzed transformation of Fe (oxyhydr)oxides across organic matter fractions in organically amended soils

Beatrice Giannetta [a], Ramona Balint [a, b], Daniel Said-Pullicino [a], César Plaza [c], Maria Martin [a], Claudio Zaccone [d]

[a] *Department of Agricultural, Forest and Food Sciences, University of Torino, Largo Paolo Braccini 2, 10095 Grugliasco, Italy*

[b] *Institute of Geosciences and Earth Resources, National Research Council of Italy (CNR), Via Valperga Caluso 35, 10125 Turin, Italy*

[c] *Instituto de Ciencias Agrarias, Consejo Superior de Investigaciones Científicas, Serrano 115 bis, 28006 Madrid, Spain*

[d] *Department of Biotechnology, University of Verona, Strada Le Grazie 15, Verona, 37134, Italy*

Corresponding author. E-mail address: beatrice.giannetta@unito.it

Abstract

The Fe(II)-catalyzed transformation of ferrihydrite into highly crystalline forms may represent an important pathway for soil organic matter (SOM) destabilization under moderately reducing conditions. However, the link between redox-driven changes in soil Fe mineral composition and crystallinity, and SOM chemical properties in the field remains elusive. We evaluated abiotic Fe(II)-catalyzed mineralogical transformation of Fe (oxyhydr)oxides in bulk soils and two particle-size SOM fractions, namely the fine silt plus clay (< 20 μm, FSi+Cl) and fine sand (50-200 μm, FSa) fractions of an agricultural soil unamended or amended with biochar, compost, or the combination of both. After spiking with Fe(II) and incubating for 7 days under anoxic and sterile conditions at neutral pH, the FSa fractions (Fe(II):Fe(III) molar ratios ≈ 3.3) showed more significant ferrihydrite transformations with respect to FSi+Cl fractions (Fe(II):Fe(III) molar ratios ≈ 0.7), with the consequent production of well-ordered Fe oxides in most soils, particularly those unamended or amended with biochar alone. Nonetheless, poorly crystalline ferrihydrite still constituted about 45% of the FSi+Cl fractions of amended soils after reaction with Fe(II), which confirms that the higher SOM and clay mineral content in this fraction may possibly inhibit atom exchange between aqueous Fe(II) and the solid phase. Building on our knowledge of abiotic Fe(II)-catalyzed mineralogical changes, the suppression of ferrihydrite transformation in FSi+Cl fractions in amended soils could ultimately lead to a slower turnover of ferrihydrite, possibly preserving the carbon sequestration potential associated with this mineral. Conversely, in both bulk soils and FSa fractions, the extent to which mineral transformation occur seemed to be contingent on the quality of the amendment used.

Keywords: EXAFS, linear combination fitting, physical fractionation, organic amendments.

1. Introduction

Soil organic carbon (SOC) cycling is strongly linked to the biogeochemical cycling of redox-active minerals, particularly iron (Fe) oxides and (oxy-)hydroxides (hereafter referred to as Fe oxides) (Lalonde et al., 2012; Kramer and Chadwick, 2018; Hemingway et al., 2019; Nguyen et al., 2019). These mineral phases serve both as important sorbents involved in the chemical stabilization of SOC due to their high affinity for binding organic matter (OM) and large specific surface area (SSA), and as major alternative electron acceptors for metabolic OM mineralization in the absence of oxygen (Schwertmann and Cornell, 2000; Kaiser et al., 2007; Hochella et al., 2008; Borch et al., 2010). Under anoxic conditions the reductive dissolution of Fe(III) oxides may influence the properties of Fe oxide phases (*e.g.*, stability, surface area) with important implications on soil OM (SOM) stabilization and turnover, although the mutual interactions between Fe and SOM cycling are not fully understood.

The release of soluble Fe(II) can subsequently contribute to the formation of a variety of secondary minerals including Fe(II), Fe(III) or mixed valence Fe(II/III) minerals (Borch et al., 2010). Furthermore, the presence of aqueous Fe(II) may catalyze the transformation of poorly-crystalline Fe(III) oxides to thermodynamically more stable phases (Stumm and Sulzberger, 1992; Pedersen et al., 2005; Yee et al., 2006; Boland et al., 2014; Tomaszewski et al., 2016; Aeppli et al., 2019). In particular, increasing aqueous Fe(II) concentrations may accelerate the transformation of ferrihydrite to substantially more crystalline lepidocrocite, goethite and magnetite. For example, it was demonstrated that at low Fe(II) concentrations (<1.0 mmol Fe(II)/g ferrihydrite), ferrihydrite was transformed to lepidocrocite and goethite, while at higher Fe(II) concentrations (>1.0 mmol Fe(II)/g ferrihydrite) the formation of magnetite was favored (Hansel et al., 2005).

Various studies have explored how OM influences Fe(II)-catalyzed ferrihydrite mineral transformation in reducing environments (Jones et al., 2009; Henneberry et al., 2012; Chen et al., 2015; Bhattacharyya et al., 2018; ThomasArrigo et al., 2018; Zhou et al., 2018; Tamrat et al., 2019). The presence of OM coatings on Fe oxides with a low crystalline order are known to inhibit the Fe(II)-catalyzed transformation to more stable and crystalline forms, due to a decrease in atom exchange between aqueous Fe(II) and Fe(III) mineral surfaces (Zhou et al., 2018). It is generally accepted that the association with OM retards Fe(III) crystallization processes (known as Ostwald ripening) by blocking dissolution sites on the Fe(III) mineral or hindering nucleation of more stable Fe(III) mineral phases (Schwertmann and Thalmann, 1976). With the use of Fe isotopes, mineral surface sites on ferrihydrite-OM coprecipitates were shown to be not completely blocked, and electron transfer and solid-phase dissolution may occur, although the presence of OM hindered crystalline mineral formation (ThomasArrigo et al., 2017, 2018, 2019; Zhou et al., 2018). Chen et al. (2015) showed that ferrihydrite coprecipitated with different amounts of a carboxylic-rich OM extracted from fresh litter samples from the O horizon of an Ultisol (C:Fe molar ratio = 0−1.6) displayed a linear decrease in mineral transformation rates with increasing C concentrations. Similarly, ThomasArrigo et al. (2017) found that carbohydrate-dominated OM fractions in freshwater flocs stabilize Fe minerals against Fe(II)-catalyzed transformation of ferrihydrite into more crystalline phases.

The kinetics of Fe recrystallization and transformation processes under changing redox conditions have been mostly studied in reductionist model systems involving dissolved organic matter (DOM) (Daugherty et al., 2017), SOM-ferrihydrite precipitates (Zhou et al., 2018), ferrihydrite-humic acids coprecipitates (Shimizu et al., 2013), freshwater flocs (ThomasArrigo et al., 2017) or soil slurries (Chen et al., 2018), but

rarely in more complex, bulk soils. Moreover, it remains less clear how Fe phase transformations relate to the quantity and chemistry of SOM under field conditions (rather than in reductionist model systems), and insights regarding these interactions across different SOM pools remain scarce. These insights can be particularly important when considering that variations in rainfall patterns due to climate change can even cause fine textured arable soils, not normally exposed to redox cycling, to experience short periods of water saturation following intense storms, therefore leading to changes in redox conditions.

The application of organic amendments to arable soils represents an important input of OM that can modify the physical and chemical conditions related to mineral stability, affecting the reactive surfaces of organo-mineral complexes, and leading to the dissolution and/or formation of mineral phases (Basile-Doelsch et al., 2009; Xiao et al., 2016). This still leaves several open questions about the influence of Fe species and abundance on SOM stability and turnover (Hall et al., 2018; Giannetta et al., 2019a), especially in agricultural soils which are commonly amended with different organic products (including biochar and compost) (Ngo et al., 2016; Plaza et al., 2016).

Based on these considerations, the objectives of this work were (1) to determine the effect of different organic amendments (*i.e.*, biochar and municipal soil waste compost applied separately or together) on the Fe(II)-catalyzed transformation of Fe(III) minerals in an arable soil, and (2) to investigate the influence of Fe-OM associations on mineral transformations across different SOM pools. We hypothesized that abiotic Fe phase transformations under simulated temporary anoxia in organically amended soils is limited by the higher SOM content resulting from the addition of exogenous OM, particularly in the finer fractions where strong Fe-OM associations are more likely to inhibit Fe atom exchange kinetics. Particle-size fractionation is a valuable tool to

separate distinct SOM pools characterized by different organo-mineral functional units. Moreover, by combining the incubation of soils with aqueous Fe(II), physical fractionation techniques and synchrotron-based Fe extended X-ray absorption fine structure (EXAFS) spectroscopy we provide insights into Fe(II)-catalyzed mineralogical transformations of Fe oxides as a function of OM quantity and quality.

2. Materials and methods

2.1. Soil sample collection and physical fractionation

The field experiment selected for this research is located in the experimental farm "La Poveda" (Spanish National Research Council, CSIC), Arganda del Rey, Madrid, Spain (3° 29′ 06″ W, 40° 18′ 58″N, 534 m above sea level). The experimental site has a Mediterranean climate, an average annual rainfall of 436 mm and average annual temperature of 14 ºC. The soil has a clay loam texture, a pH of 8.4 and is classified as a Xerofluvent (Soil Survey Staff, 2014). For this work, we used topsoil samples (0-15 cm) collected in late June 2013, from the plots unamended (UN) and amended in late October 2012 with biochar (BC), municipal solid waste compost (MC) and both (BC+MC). The experiment design and the main properties of the soil and amendments are reported in Plaza et al. (2016) and summarized in Table 1.

A physical size fractionation by ultrasonic dispersion and wet sieving was performed, allowing for the separation of particles into four different size fractions: coarse sand (CSa: 2000-200 µm diameter), fine sand (FSa: 200-50 µm), coarse silt (CSi: 50-20 µm) and fine silt and clay (FSi+Cl: <20 µm) (Lopez-Sangil and Rovira, 2013; Giannetta et al., 2019b). Briefly, 15 g of each sample were transferred into 50 mL vials and suspended in 30 mL deionized water. Samples were then subjected to vertical agitation (20 rpm) for 60 minutes and to ultrasonic dispersion with an energy input of

1020 J mL^{-1} (Branson 45 Sonifier, Branson Ultrasonics Corporation, Danbury, USA). The suspensions were then wet-sieved through a set of three sieves (200 µm, 50 µm and 20 µm mesh). The fractions retained by sieves (CSa, FSa, CSi respectively) were directly recovered from the sieves, quantitatively transferred to pre-weighted vials and dried at 60 ºC to constant weight. The particles passing through the last sieve (<20 µm: FSi+Cl) were brought to 1 L with water, flocculated by adding 2 mL of saturated potassium aluminium sulfate solution, and the suspension left to settle at 4°C for 2 days, until complete sedimentation of the solid particles. The overlying water was siphoned off and discarded. The sediment was recovered by centrifugation (15 min at 2500×g), transferred to a pre-weighed flask and dried at 60 ºC to constant weight.

Total organic C and N contents were determined by dry combustion (Flash 2000 NC Analyzer Thermo Scientific, Bremen, Germany). Each sample was ground with a ball mill and subjected to acid fumigation before analysis to remove carbonates (Harris et al., 2001). Pseudo-total Fe concentrations in soil and amended samples were determined by inductively coupled plasma - optical emission spectrometry (ICP-OES, iCAP 6500, Thermo Fisher Scientific, MA) after digestion with nitric and perchloric acid (Faithfull, 2002).

X-ray diffraction (XRD) patterns of the soil fractions were reported in Giannetta et al. (2020a). The FSa and FSi+Cl fractions showed a similar composition in terms of main mineral phases, with some differences in terms of relative percentages. In particular, quartz was much more abundant in the FSa (67−76%) compared to the FSi+Cl (34−58%), as expected, whereas muscovite was higher in FSi+Cl (8−15%) versus FSa (2−4%). Smaller differences between the two fractions was observed also for calcite and chlorite.

2.2. Incubation of soils and size fractions with Fe(II)

Fe(II) spiking and anaerobic incubation was used to study the abiotic Fe(II)-catalyzed mineral transformations in bulk soils and size fractions. In this work, we only focused on two of the four size fractions separated, namely the FSi+Cl and FSa fractions, that represented chemically and functionally distinct SOM pools. The <20 μm size-fraction is generally responsible for the greatest proportion of mineral-associated SOM stabilized through strong binding to mineral surfaces through polyvalent cation bridging and ligand-exchange with Al and Fe oxides (von Lützow et al., 2006). On the other hand, the coarser 200-50 μm fraction is characterized by particulate OM and a mineral phase with low surface area and charge, and thus less relevant for organic C partitioning in soils (Six et al., 1998). Nevertheless, it has been shown that also sand particles can be coated with Fe oxides through electrostatic forces, Van der Waals interactions, and Fe-O-Si bonds (Scheidegger et al., 1993), with consequences on the SSA (Giannetta et al., 2019a), adsorption phenomena and cation exchange capacity.

Dried sample material (100 mg) was placed in crimp-top serum vials and suspended in 25 mL deionized water in duplicate. After adjusting the pH of the suspensions to 7.0 ± 0.1 with 0.1 or 0.01 M NaOH or HNO_3, anoxic 3-(*N*-morpholino) propanesulfonic acid (MOPS) buffer (Sigma-Aldrich, St. Louis, USA) adjusted to pH 7 was added to obtain a final concentration of 50 mM and a final volume of 50 mL. The vials were immediately sealed and the headspace purged with N_2. Chloroform (50 μL) was added to inhibit biotic reactions, the vials were transferred into a glovebox (100% N_2 atmosphere) for subsequent handling. After 16 h equilibration, the samples were spiked with 0.5 mL of 100 mM $FeCl_2 \cdot 4H_2O$ (Sigma-Aldrich, St. Louis, USA) to reach a final Fe^{2+} concentration in the vials of 1 mM Fe(II), and incubated in the dark for 7 days. Preliminary experiments showed that the pH remained at 7.0 ± 0.3 throughout the

duration of the experiment and was no longer monitored during the incubation. Fe(II)-free controls were included for each treatment to quantify Fe release and exclude microbially-driven solid-phase dissolution during the incubation. Material for solid-phase analysis was collected on 0.22-μm cellulose filters, thoroughly rinsed with anoxic deionized water, and dried always in the glovebox atmosphere. Finally, samples were homogenized with a pestle and mortar, and kept anoxic until further analyses.

2.3. Iron K-edge extended X-ray adsorption fine structure (EXAFS) spectroscopy

X-ray absorption spectroscopic (XAS) analyses of bulk, FSa and FSi+Cl fractions before and after Fe(II) spiking were carried out at the XAFS beamline at Elettra Sincrotrone (Trieste, Italy) (Di Cicco et al., 2009; Aquilanti et al., 2017). Fe(II)-reacted samples were prepared as pressed powders (*ca.* 15 mg) between Kapton® tape under anoxic conditions in a glovebox, and kept anoxic until the end of the XAS measurements. Fe EXAFS spectra were recorded in transmission mode using Si (111) monochromator, which was calibrated to the first-derivative maximum of the K-edge absorption spectrum of a metallic Fe foil (7112 eV). The monochromator was detuned 40% to reduce higher order harmonics. Two to six scans were collected and averaged to increase the signal-to-noise ratio.

As previously described in Giannetta et al. (2020a, b), a suite of linear combination fitting (LCF) techniques designed to identify the major Fe components in the studied samples by comparison with the spectra of well characterized standards, was employed to analyze the synchrotron-based data. Additional methods for synchrotron-based data acquisition and analysis, including Principal Component Analysis (PCA) (Table S1 and Figure S1), Target Transformation (TT), SPOIL values (Table S2), LCF of EXAFS

data, as well as a description of the standards used, are reported as Supplementary Information.

3. Results

3.1. Organic C and total N contents in the fractions

The FSa and FSi+Cl fractions accounted for about 26% and 39% of the mass of the soils, respectively, regardless of the amendment treatment. The organic C and N contents of the FSa and FSi+Cl pools of the soils examined here have been reported in a previous work (Giannetta et al., 2020a). Briefly, on average, the FSi+Cl fractions showed much higher organic C (23.1 g kg^{-1}), smaller C/N ratios (10.8) and higher Fe contents (39.6 g kg^{-1}) with respect to the FSa fractions (mean 6.4 g C kg^{-1}, C/N = 18.2, 8.6 g Fe kg^{-1}) across treatments (Table 2). Moreover, the organic C and Fe contents in the FSi+Cl and FSa fractions represented 47-60% and 8-11% of the total SOC, and 67-73% and 9-11% of the total Fe, respectively. Irrespective of the type of amendment, the FSi+Cl fraction also accounted for most of the total N in the studied soils. The large C/N ratios of the FSa fraction (ranging from 13.5 in the UN soil to 24.8 in the BC soil) suggest that OM in this fraction can be characterized by relatively recent particulate OM, and not involved in chemical interactions with the mineral phase. This is consistent with a previous work by Plaza et al. (2016) that showed that biochar accumulated in mineral-free light SOM fractions.

For both fractions, the lowest organic C, total N contents and C/N ratios were observed for UN, whereas the soil amended with BC+MC showed highest values (Giannetta et al., 2020a). For both FSa and FSi+Cl fractions, organic C and total N contents followed the order BC+MC > BC > MC > UN.

3.2. Solid-phase mineral analysis: Fe EXAFS

3.2.1. Qualitative Fe speciation in bulk and size-fractions

The qualitative speciation of Fe in the bulk soils and size-fractions by Fe K-edge EXAFS was carried out by comparison with several standards (Figure 1). Fe(III)-citrate is generally used as an analog model compound for Fe(III)-OM complexes because it consists of Fe bound directly to organic C (O'Day et al., 2004). Low molecular weight organic acids represent naturally occurring organic ligands originating as microbial metabolites and root exudates, and constitute an important part of labile C associated with Fe oxides (Yang et al., 2016). Fe K-edge EXAFS spectra showed features at ~4.0 $Å^{-1}$ (maximum 1), ~6.5 $Å^{-1}$ (maximum 2), ~7.5 $Å^{-1}$ (maximum 3), ~8.5 $Å^{-1}$ (maximum 4) (Figure 1). The maximum at 4.0 $Å^{-1}$ has different features in ferrihydrite and lepidocrocite (Figure 1). The maximum at 7.5 $Å^{-1}$ is characteristic of ferrihydrite, whereas the small maximum at 8 $Å^{-1}$ is typical of lepidocrocite and magnetite, and a broad one describes Fe(III)-citrate spectrum representing Fe(III)-OM complexes where Fe is directly bound by carboxylic functional groups (Figure 1). The maximum at 8.5 $Å^{-1}$ is also a characteristic feature of ferrihydrite. The maximum at 10 $Å^{-1}$ is only characteristic of lepidocrocite (Figure 1).

PCA analysis of the soils (Figure S1) indicated that a maximum of four spectra were needed to reconstruct the EXAFS data. A scree plot was employed, where a break in the slope of the scree plot indicates the minimum number of components in the system. The scree plot had a slight break in the slope at four components which would again indicate that the EXAFS data can be reconstructed with a minimum of four standards. However, the major break in the slope was at two components, which indicates that a minimum of two components were necessary to adequately reconstruct the data. Based on these varied results, between two and four components were necessary to reconstruct the data.

Considering three standards, the Fe speciation of UN bulk soils evidenced the presence of lepidocrocite, Fe(III)-citrate, and chlorite (Figure 2; Table S3). With an additional component, the fitting improved only for the BC+MC soil (Figure S2; Table S3). The spectra of all the other amended bulk soils were accurately reconstructed by three components (Figure 2). In no case the use of only two standards was found to have I values <0.05. The F-test results proved that visual inspection of the components and the scree plot (Figure S1) may not suffice to determine the significant number of standards to include in the fit. Structurally important features should be captured when the fit is statistically improved. For example, for the BC soil the F-test (I = 0.0022) determined that the fit only needed three standards. The best fit using three standards captured structurally relevant features, as the fit line closely match the real data at 8.5 $Å^{-1}$, typical of ferrihydrite (Figure 2). On the other hand, the fit line was closer to the real data using four standards instead of three (Figure S2). When spiked with Fe(II) at pH 7, defined maxima at 4.0 $Å^{-1}$, as also the one around 6.5 $Å^{-1}$ attributed to crystalline lepidocrocite appeared in the UN bulk soil. This was also evident, to a lesser extent, in the BC+MC samples. Additionally, the maxima at 8 and 10 $Å^{-1}$ confirmed the presence of lepidocrocite in the UN sample (Figure 2). On the other hand, MC and BC soils presented the maxima typical of ferrihydrite (Figure 2).

For all spectra relative to the FSa size-fractions across treatments, F-tests confirmed that fitting components corresponding to experimental spectra of model compounds were adequately described using three components (Figure 3, Table S4). Considering three standards, the FSa fraction of the UN soil was characterized by the presence of lepidocrocite, Fe(III) citrate, and chlorite (Figure 3, Table S4), but including an additional component still maintained the fitting statistically valid (Figure S3, Table S4), resulting in a contribution of both crystalline lepidocrocite and magnetite to the Fe

oxides components. For all amended soils, the I value of the FSa fractions was always < 0.05, using three components instead of four. In the MC soil, the formation of more crystalline Fe oxides was not noticeable in the FSa fraction, and ferrihydrite still represented the main component (Table S4). In the BC soil, the presence of ferrihydrite was no longer detected while maxima typical of lepidocrocite at 4.0 $Å^{-1}$, at *ca.* 6 $Å^{-1}$, also typical of magnetite and at 10 $Å^{-1}$ were observed (Figure 3). An intermediate situation occurred for the BC+MC soil, where the presence of both ferrihydrite and lepidocrocite were observed (Figure 3). All FSa fractions contained relatively low amount of OM associated to Fe(III), from 22% in UN to 42% in BC+MC (Table S4).

The R-factors in all the FSi+Cl fraction demonstrated that the fits obtained using three and four components were equivalently good (Figures 3 and S3). However, considering four instead of three components for the FSi+Cl fraction of the UN soils improved the fitting and evidenced a substantial contribution from ferrihydrite (Figure S3), apart from Fe(III)-citrate, chlorite and lepidocrocite (Figures 3 and S3). Similarly, the reconstruction using four components evidenced the presence of both ferrihydrite and lepidocrocite in the FSi+Cl fraction of the MC soil. In contrast, spectra of the fine fraction from the BC and the BC+MC soils, adequately described using three components, did not evidence the presence of lepidocrocite (Figure 3). Fe (III)-citrate represented a main constituent of all FSi+Cl fractions across treatments (*ca.* 40%).

Comparing spectra for FSi+Cl and FSa fractions (Figure 3), the maxima found in the latter at *ca.* 6 $Å^{-1}$ and at 10 $Å^{-1}$ were attenuated and not detected, respectively. In all the FSi+Cl fractions the maximum at 4 $Å^{-1}$ reveals features most similar to the ferrihydrite and not the lepidocrocite spectra, thus indicating that in only in the FSa fractions a transformation of ferrihydrite into lepidocrocite occurred.

3.2.2. Solid-phase mineral transformation after Fe(II) addition

The composition of Fe phases in bulk soils before Fe(II) treatment were mainly characterized by Fe(III) oxides, Fe(III)-OM, and chlorite when using both three and four components to describe the fit. After incubation with Fe(II), lepidocrocite represented the main Fe oxide phase in the UN soil (66%) with lower proportions of Fe(III)-citrate (22%) and chlorite (16%). In contrast, in MC and BC soils, ferrihydrite represented the main component (44 and 42%, respectively) after Fe(II) treatment, while the proportion described by Fe(III)-citrate was higher with respect to the UN soil (39 and 35%, respectively). Fe phase speciation in the BC+MC soil after incubation with Fe(II), more adequately explained using four components, evidenced important contributions from both lepidocrocite (36%) and ferrihydrite (16%) to the Fe oxide composition (Table S3).

In a previous study (Giannetta et al., 2020a), Fe K-edge EXAFS was adopted to identify and quantify the Fe phases present in the same fractions (FSa and FSi+Cl) prior to incubation with Fe(II). In the UN soil, the FSa fraction contained Fe species characterized by ferrihydrite (44%), followed by chlorite (26%) and with a lower contribution from Fe(III)-citrate (18%). Reaction with Fe(II) led to the disappearance of ferrihydrite present in this size-fraction and the appearance of lepidocrocite that constituted 67% of the Fe phases, with little or no change in the contribution of chlorite and Fe(III)-citrate forms (Figure 4a). In the MC soil, reaction of the FSa fraction with Fe(II) led to a slight increase in ferrihydrite from 28 to 38%, without transformation into a more crystalline phase (Figure 4a). In the BC soil, the proportion of ferrihydrite (29%) originally present in this size-fraction was no longer detected after incubation with Fe(II), while significant proportions of lepidocrocite (53%) and magnetite (11%) were observed (Figure 4a). In the BC+MC soil, the proportion of ferrihydrite in the FSa fraction decreased from 28 to 19% after incubation with Fe(II), while the appearance of

lepidocrocite (17%) was observed (Figure 4a). Moreover, the contribution of Fe(III)-citrate increased from 35 to 41% (Figure 4a, Table S4). The disappearance of chlorite after incubation with Fe(II) in both BC and BC+MC soils was probably due to a "dilution effect" to below quantification levels caused by the formation of new Fe phases during the incubation involving part of the added Fe(II).

Fe (II)-catalyzed transformation of Fe phases in the FSi+Cl fractions showed different trends with respect to the FSa fractions. Before incubation with Fe(II) the composition of Fe phases in the finer size-fraction were rather similar across treatments, and mainly characterized by ferrihydrite (45-48%) and Fe(III)-citrate (37-44%) with minor proportions of chlorite (18-22%) (Figure 4b). After incubation with Fe(II) the proportion of ferrihydrite in the FSi+Cl fractions of the UN and MC soils decreased to 31 and 33%, respectively, while small proportions of lepidocrocite (17%) were detected (Figure 4b). In contrast, no significant differences were observed in the Fe phase composition of the FSi+Cl fraction of BC and BC+MC soils after incubation with Fe(II) (Figure 4b).

4. Discussion

4.1. Fe mineral transformations in bulk amended soils

Under anaerobic conditions Fe(II)-catalyzed transformation of ferrihydrite can lead to the formation of Fe oxides with a higher degree of order as a function of the concentration of dissolved Fe(II) and the presence of OM (Jeon et al., 2003; Hansel et al., 2004, 2005; Pedersen et al., 2005; Liu et al., 2007; Yang et al., 2010; Latta et al., 2012; Usman et al., 2012; Boland et al., 2014). Our hypothesis that abiotic Fe phase transformations under simulated temporary anoxia in organically amended soils is limited by the higher SOM content resulting from the addition of exogenous OM was

confirmed. Higher organic C contents with amendment seem to be responsible of the decreased extent of Fe(II)-induced abiotic ferrihydrite transformation in bulk soils, such that ferrihydrite still represented the main Fe oxide component in the BC+MC amended but not in the unamended soils after incubation with Fe(II). Jones et al. (2009) found that 25 or 150 mg L^{-1} of DOM (Suwannee River fulvic acid) effectively hindered the Fe(II)-catalyzed transformation of ferrihydrite and lepidocrocite. Although increasing contents of OM can be generally assumed to reduce the reactivity of Fe oxide surfaces towards Fe(II), mineral transformations observed in bulk soils may not effectively represent the changes that occur in different functional SOM pools.

By adopting particle-size fractionation procedures, the coarser fractions primarily characterized by particulate OM with a faster turnover (higher C/N) and not involved in chemical interactions with the mineral phase are distinguished from the finest soil fractions generally characterized by clay minerals with a higher Fe content and OM with a slower turnover (lower C/N), stabilized by chemical interaction with mineral surfaces.

4.2. Fe mineral transformations in the coarse OM fractions

The FSa size fraction of the UN soil contained the highest percentage of lepidocrocite after treatment with Fe(II) possibly due to the Ostwald ripening of ferrihydrite (Schwertmann and Cornell, 2000), caused by the dissolution and reprecipitation of ferrihydrite to lepidocrocite (Hansel et al., 2005). Although this fraction only represented a small proportion of the total SOM and Fe content, the limited interaction between these two components allowed for significant Fe(II)-catalyzed transformation of the Fe oxides present.

Amendment with compost prevented the transformation of ferrihydrite into more stable Fe oxides. During composting, the decrease in water-extractable organic C can be assigned to the degradation of the most labile soluble organic moieties, particularly carbohydrates, amino sugars and low-molecular-weight organic acids, while the soluble organic fraction present in the final compost is rich in carboxyl groups and aromatic moieties considered characteristic of the stabilization process (Said-Pullicino et al., 2007). Notwithstanding the relatively high Fe(II):Fe(III) molar ratio (≈ 3.1) during incubation, the binding of the added Fe(II) with the carboxyl-rich aromatic groups typical of compost is the most likely explanation for the inhibition of ferrihydrite transformation to more crystalline forms.

In contrast, although the coarse particle-size fraction separated from the BC soil had a significantly higher organic C content with respect to similar fractions obtained from the UN or MC soils, incubation with Fe(II) led to the disappearance of ferrihydrite and formation of both magnetite and lepidocrocite, suggesting that the conditions for ferrihydrite Fe(II)-catalyzed transformations were not impaired by the presence of OM. We hypothesize that the presence of magnetite and lepidocrocite in this FSa fraction amended with biochar was possibly due to the combination of the relatively high Fe(II):Fe(III) molar ratio, the neutral pH at which incubation was carried out, as well as the role of aromatic constituents of biochar in mediating electron transfer processes thus favouring the transformation of the Fe(III) oxyhydroxide (Kappler et al., 2014). It has been demonstrated that biochar contains aromatic and quinone functionalities, through which this material can participate in environmentally relevant biotic and abiotic redox reactions (Kappler et al., 2014; Klüpfel et al., 2014; Yuan et al., 2017). Related to the quality of the organic amendments, diffuse reflectance infrared Fourier transform (DRIFT) spectra recorded in previous work confirm that biochar is more aromatic than

compost (Plaza et al., 2016). Biochar redox reactions were previously reported to involve (i) redox cycling via redox active quinone/hydroquinone groups (Kappler et al., 2014), (ii) storage and release of electrons via the electrical double-layer capacitance of C matrices (Sun et al., 2017), and (iii) direct electron transfer through the electrical conductance of C matrices (Sun et al., 2017, 2018; He et al., 2019) The results reported in Yang et al. (2020) suggested that, for ferrihydrite reduction, a certain biochar particle-size and biochar/ferrihydrite ratio is necessary, leading to a close aggregation of all phases. This aggregation, possibly occurring in the separated fraction, favors electron transfer to ferrihydrite via redox cycling of the electron donating and accepting functional groups of biochar and via direct electron transfer through conductive biochar C matrices. After the amendment with both biochar and compost, only the formation of lepidocrocite occurred, thus underlining an intermediate situation between the soils amended with only biochar or compost.

4.3. Fe mineral transformations in the fine OM fractions

Compared to the coarser fractions in which Fe phase transformations were strongly dependent on organic amendment, ferrihydrite transformations in the finer fraction of amended soils were generally inhibited, and only the unamended soil showed a minor degree of transformation into lepidocrocite. These results suggest that the addition of exogenous OM can effectively impair the Fe(II)-catalyzed transformation of ferrihydrite in the fine, but not necessarily in the coarse, particle-size SOM fractions.

Several mechanisms may explain the different behaviour of the different size fractions. First, the adsorption or coprecipitation of OM with Fe(III) oxides in the fine fraction could have resulted in a decrease in available sorption sites for Fe(II). With increasing surface coverage (*i.e.*, increasing C/Fe molar ratios), the decrease in SSA and

porosity of ferrihydrite-OM associations would hinder aqueous Fe(II) from adsorbing to and transferring electrons to ferrihydrite (Boland et al., 2012; Chen et al., 2015). Nonetheless, nearly complete atom exchange was reported to occur in ferrihydrite–OM coprecipitates at C/Fe molar ratios of 2.5, suggesting that not all surface sites are blocked, even though the presence of OM hindered crystalline mineral formation (ThomasArrigo et al., 2018). The C/Fe molar ratios of the fine fractions in this work ranged from 2.2 for the unamended soil to 2.9-3.1 for the organically amended soils. This probably explained why ferrihydrite transformations in this fraction were observed for the unamended but not for the organically amended soils.

Secondly, the higher Fe content of the FSi+Cl fraction with respect to the coarser fraction (Table 2) resulted in lower Fe(II):Fe(III) molar ratios during incubation (on average 0.7 and 3.3, respectively). It is well recognized that Fe(II):Fe(III) molar ratios influence the rates and products of mineral transformations in both pure mineral systems and in the presence of OM (Hansel et al., 2011; Boland et al., 2014; Chen et al., 2015; ThomasArrigo et al., 2017, 2018). Thus, it is likely that fewer mineral transformations were generally observed in the finer fractions as a direct result of the lower Fe(II):Fe(III) ratios. Nonetheless, Fe(II)-catalyzed ferrihydrite transformations have been shown to occur even at significantly lower molar ratios (Hansel et al., 2005; Boland et al., 2014; Zhou et al., 2018), suggesting that transformations in the FSi+Cl fraction were not necessarily limited by this low ratio. Moreover, within the same size fractions, Fe(II):Fe(III) ratios were rather comparable, and not assumed to be responsible for the observed differences in Fe phase transformations between soils. In general, Fe(II)/Fe(III) ratio seem to have a large influence on the secondary Fe minerals formed, with higher Fe(II) concentrations leading to goethite and magnetite, whereas

lepidocrocite prevalently formed at lower Fe(II) concentrations (Hansel et al., 2005; Boland et al., 2014).

In addition, abiotic reactions between aqueous Fe(II) and structural Fe(III) within clay minerals, involving Fe(II)-Fe(III) redox-cycling, could have also played an important role in determining Fe phase transformations. It is known that Fe-containing and Fe-poor phyllosilicates participate in Fe(II)-catalyzed electron transfer (Schaefer et al., 2011; Zhu and Elzinga, 2014; Neumann et al., 2015; Latta et al., 2017). Fe(II) sorption to Fe-bearing clay minerals followed by electron transfer to structural Fe(III) may result in the formation of an Fe(II)-containing clay mineral and a solid Fe oxidation product (Schaefer et al., 2011; Zhu et al., 2018). Schaefer et al. (2011) provided evidence that Fe(II) adsorbed by nontronite reduces structural Fe(III) within the clay, with sorbed Fe(II) being oxidized to lepidocrocite. Neumann et al. (2015) found that the Fe(II)-to-Fe(III) electron hopping frequency within the octahedral sheet of nontronites to be significant even at room temperature. Thus, bulk electron conduction through the octahedral sheet may connect Fe(II) oxidation at one surface site of clay minerals with reductive dissolution of structural Fe(III). It seems therefore plausible that, in our study, the added Fe(II) could have partially reacted with the abundant clay minerals present in the fine fraction rather than with ferrihydrite, partly contributing to the observed lack of transformations in Fe phase composition.

Although these mechanisms may explain the differences in Fe phase transformations between coarse and fine soil fractions, the presumably similar clay mineralogy and similar Fe(II):Fe(III) molar ratios in the FSi+Cl fraction across the different soils point to a predominant effect of OM content and quality in limiting Fe(II)-catalyzed transformations in finer fractions of organically amended with respect to unamended soils.

5. Conclusions

The combined use of Fe EXAFS and size-fractioned samples represents an important approach to study Fe dynamics and the transformation of Fe(III) oxides in natural environments. Our results on Fe(II)-catalyzed mineral transformations in unamended and organically amended bulk soils and particle-size SOM fractions allowed us to constrain the possible mechanisms through which SOM can affect the formation of more crystalline Fe minerals. Finer soil fractions were less susceptible to redox-driven abiotic Fe phase transformations due their higher OM and clay mineral contents with respect to coarser fractions, with both Fe oxide surface passivation by sorbed OM and Fe(II) sorption to Fe-bearing clay minerals potentially contributing to limiting the Fe(II)-catalyzed transformation of Fe oxides with a low crystalline order. On the other hand, Fe oxide transformations and their relation to the type of organic amendment were more evident in coarser particle-size fractions, suggesting that this fraction could represent an understudied pool of SOM subject to Fe mineral transformations.

Understanding the factors controlling the transformation of Fe(III) (oxyhydr)oxides across SOM fractions *in situ* is of particular environmental relevance as this has implications on mutual interactions between organic C and Fe cycling under differently managed soils, and may serve to establish management regimes which help maximize the environmental sustainability of agricultural practices.

Acknowledgements

We thank Pere Rovira (Forest Sciences Centre of Catalonia) for the help during physical fractionation, Peggy O'Day (University of California Merced) and all the co-authors of the O'Day et al. (2004) paper, Ellen E. Daugherty (Colorado State University) and all

the co-authors of the Daugherty et al. (2017) paper for providing the spectra of the standards used for the LCF. We acknowledge ELETTRA for the provision of synchrotron radiation facilities in the framework of proposal n. 20185454 and thank Giuliana Aquilanti, Luca Olivi, and Danilo Olivera De Souza (ELETTRA, XAFS beamline), for their support during the synchrotron measurements. C.P. acknowledges support from the Spanish State Plan for Scientific and Technical Research and Innovation 2013-2016 (AGL201675762-R, AEI/FEDER, UE).

References

Aeppli, M., Kaegi, R., Kretzschmar, R., Voegelin, A., Hofstetter, T.B., Sander, M., 2019. Electrochemical analysis of changes in iron oxide reducibility during abiotic ferrihydrite transformation into goethite and magnetite. Environ. Sci. Technol. 53, 3568–3578.

Aquilanti, G.; Giorgetti, M., Dominko, R., Stievano, L., Arčon, I., Novello, N., Olivi, L., 2017. *Operando* characterization of batteries using x-ray absorption spectroscopy: Advances at the beamline XAFS at synchrotron Elettra. J. Phys. D. Appl. Phys. 50, 074001.

Basile-Doelsch, I., Brun, T., Borschneck, D., Masion, A., Marol, C., Balesdent, J., 2009. Effect of landuse on organic matter stabilized in organomineral complexes: A study combining density fractionation, mineralogy and $\delta^{13}C$. Geoderma 151, 77–86.

Bhattacharyya, A., Campbell, A.N., Tfaily, M.M., Lin, Y., Kukkadapu, R.K., Silver, W.L., Nico, P.S., Pett-Ridge, J., 2018. Redox fluctuations control the coupled cycling of iron and carbon in tropical forest soils. Environ. Sci. Technol. 52, 14129–14139.

Boland, D.D., Collins, R.N., Miller, C.J., Glover, C.J., Waite, T.D., 2014. Effect of solution and solid-phase conditions on the Fe(II)-accelerated transformation of ferrihydrite to lepidocrocite and goethite. Environ. Sci. Technol. 48, 5477–5485.

Borch, T., Kretzschmar, R., Kappler, A., Van Cappellen, P., Ginder-Vogel, M., Voegelin, A., Campbell, K., 2010. Biogeochemical redox processes and their impact on contaminant dynamics. Environ. Sci. Technol. 44, 15–23.

Chen, C., Kukkadapu, R., Sparks, D.L., 2015. Influence of coprecipitated organic matter on $Fe^{2+}_{(aq)}$-catalyzed transformation of ferrihydrite: implications for carbon dynamics. Environ. Sci. Technol. 49, 10927–10936.

Chen, C., Meile, C., Wilmoth, J., Barcellos, D., Thompson, A., 2018. Influence of pO_2 on iron redox cycling and anaerobic organic carbon mineralization in a humid tropical forest soil. Environ. Sci. Technol. 52, 7709–7719.

Daugherty, E.E., Gilbert, B., Nico, P.S., Borch, T., 2017. Complexation and redox buffering of iron(II) by dissolved organic matter. Environ. Sci. Technol. 51, 11096–11104.

Di Cicco, A., Aquilanti, G., Minicucci, M., Principi, E., Novello, N., Cognini, A., Olivi, L., 2009. Novel XAFS capabilities at ELETTRA synchrotron light source. J. Phys.: Conf. Ser. 190, 012043.

Faithfull, N.T., 2002. Methods in agricultural chemical analysis: a practical handbook, Centre for Agriculture and Bioscience International Publishing, Wallingford, U.K.

Giannetta, B., Zaccone, C., Plaza, C., Siebecker, M.G., Rovira, P., Vischetti, C., Sparks, D.L., 2019a. The role of Fe(III) in soil organic matter stabilization in two size fractions having opposite features. Sci. Total Environ. 653, 667-674.

Giannetta, B., Plaza, C., Zaccone, C., Vischetti, C., Rovira, P., 2019b. Ecosystem type effects on the stabilization of organic matter in soils: Combining size fractionation with sequential chemical extractions. Geoderma 353, 423-434.

Giannetta, B., Plaza, C., Siebecker, M.G., Aquilanti, G., Vischetti, C., Plaisier, J.R., Juanco, M., Sparks, D.L., Zaccone, C., 2020a. Iron speciation in organic matter fractions isolated from soils amended with biochar and organic fertilizers. Environ. Sci. Technol. 54, 5093-5101.

Giannetta, B., Siebecker, M.G., Zaccone, C., Plaza, C., Rovira, P., Vischetti, C., Sparks, D.L., 2020b. Iron (III) fate after complexation with soil organic matter in fine silt and clay

fractions: an EXAFS spectroscopic approach. Soil Till. Res. 200, 104617.

Hall, S. J., Berhe, A.A., Thompson, A., 2018. Order from disorder: do soil organic matter composition and turnover co-vary with iron phase crystallinity? Biogeochemistry 140, 93-110.

Hansel, C.M., Benner, S.G.; Nico, P., Fendorf, S., 2004. Structural constraints of ferric (hydr)oxides on dissimilatory iron reduction and the fate of Fe(II). Geochim. Cosmochim. Acta 68, 3217–3229.

Hansel, C.M., Benner, S.G., Fendorf, S., 2005. Competing Fe(II)-induced mineralization pathways of ferrihydrite. Environ. Sci. Technol. 39, 7147–7153.

Hansel, C.M., Learman, D.R., Lentini, C.J., Ekstrom, E.B., 2011. Effect of adsorbed and substituted Al on Fe(II)-induced mineralization pathways of ferrihydrite. Geochim. Cosmochim. Acta 75, 4653-4666.

Harris, D., Horwáth, W.R., van Kessel, C., 2001. Acid fumigation of soils to remove carbonates prior to total organic carbon or carbon-13 isotopic analysis. Soil Sci. Soc. Am. J. 65, 1853–1856.

He, X.S., Yang, C., You, S.H., Zhang, H., Xi, B.D.; Yu, M. Da; Liu, S. J., 2019. Redox properties of compost-derived organic matter and their association with polarity and molecular weight. Sci. Total Environ 665, 920–928.

Hemingway, J.D., Rothman, D.H., Grant, K.E., Rosengard, S.Z., Eglinton, T.I., Derry, L.A., Galy, V.V., 2019. Mineral protection regulates long-term global preservation of natural organic carbon. Nature 570, 228–231.

Henneberry, Y.K., Kraus, T.E.C., Nico, P.S., Horwath, W.R., 2012. Structural stability of coprecipitated natural organic matter and ferric iron under reducing conditions. Org. Geochem. 48, 81–89.

Hochella, M.F., Lower, S.K., Maurice, P.A., Penn, R.L., Sahai, N., Sparks, D.L., Twining, B.S., 2008. Nanominerals, mineral nanoparticles, and earth systems. Science 319, 1631–1635.

Jeon, B.-H., Dempsey, B.A., Burgos, W.D., 2003. Kinetics and mechanisms for reactions of Fe(II) with iron(III) oxides. Environ. Sci. Technol. 37, 3309–3315.

Jones, A.M., Collins, R.N., Rose, J., Waite, T.D., 2009. The effect of silica and natural organic matter on the Fe(II)-catalysed transformation and reactivity of Fe(III) minerals. Geochim. Cosmochim. Acta 73, 4409–4422.

Kaiser, K., Mikutta, R., Guggenberger, G., 2007. Increased stability of organic matter sorbed to ferrihydrite and goethite on aging. Soil Sci. Soc. Am. J. 71, 711–719.

Kappler, A., Wuestner, M.L., Ruecker, A., Harter, J., Halama, M., Behrens, S., 2014. Biochar as an electron shuttle between bacteria and Fe(III) minerals. Environ. Sci. Technol. Lett. 1, 339–344.

Klüpfel, L., Keiluweit, M., Kleber, M., Sander, M., 2014. Redox properties of plant biomass-derived black carbon (biochar). Environ. Sci. Technol. 48, 5601–5611.

Kramer, M.G., Chadwick, O.A., 2018. Climate-driven thresholds in reactive mineral retention of soil carbon at the global scale. Nat. Clim. Change 8, 1104–1108.

Lalonde, K., Mucci, A., Ouellet, A., Gélinas, Y., 2012. Preservation of organic matter in sediments promoted by iron. Nature 483, 198–200.

Latta, D.E., Gorski, C.A., Scherer, M.M., 2012. Influence of Fe^{2+}-catalysed iron oxide

recrystallization on metal cycling. Biochem. Soc. Trans. 40, 1191–1197.

Latta, D.E., Neumann, A., Premaratne, W.A.P.J., Scherer, M.M., 2017. Fe(II)-Fe(III) electron transfer in a clay mineral with low Fe content. Acs Earth Space Chem. 1, 197-208.

Liu, H., Li, P., Zhu, M., Wei, Y., Sun, Y., 2007. Fe(II)-induced transformation from ferrihydrite to lepidocrocite and goethite. J. Solid State Chem. 180, 2121–2128.

Lopez-Sangil, L., Rovira, P., 2013. Sequential chemical extractions of the mineral-associated soil organic matter: An integrated approach for the fractionation of organo-mineral complexes. Soil Biol. Biochem. 62, 57–67.

Neumann, A., Wu, L., Li, W., Beard, B.L., Johnson, C.M., Rosso, K.M., Frierdich, A.J., Scherer, M. M., 2015. Atom exchange between aqueous Fe(II) and structural Fe in clay minerals. Environ. Sci. Technol. 49, 2786-2795.

Ngo, P. T., Rumpel, C., Janeau, J.-L., Dang, D.-K., Doan, T.T., Jouquet, P., 2016. Mixing of biochar with organic amendments reduces carbon removal after field exposure under tropical conditions. Ecol. Eng. 91, 378–380.

Nguyen, M.L., Goldfarb, J.L., Plante, A.F., Lau, B.L.T., Hockaday, W.C., 2019. Sorption temperature and the stability of iron-bound soil organic matter. Geoderma 341, 93–99.

O'Day, P.A.; Rivera, N., Root, R., Carroll, S.A., 2004. X-ray absorption spectroscopic study of Fe reference compounds for the analysis of natural sediments. Am. Mineral. 89, 572–585.

Pedersen, H.D., Postma, D., Jakobsen, R., Larsen, O., 2005. Fast transformation of iron oxyhydroxides by the catalytic action of aqueous Fe(II). Geochim. Cosmochim. Acta 69, 3967–3977.

Plaza, C., Giannetta, B., Fernández, J.M., López-de-Sá, E.G., Polo, A., Gascó, G., Méndez, A., Zaccone, C., 2016. Response of different soil organic matter pools to biochar and organic fertilizers. Agric. Ecosyst. Environ. 225, 150–159.

Said-Pullicino, D., Kaiser, K., Guggenberger, G., Gigliotti, G., 2007. Changes in the chemical composition of water-extractable organic matter during composting: Distribution between stable and labile organic matter pools. Chemosphere 66, 2166–2176.

Schaefer, M.V., Gorski, C.A., Scherer, M.M., 2011. Spectroscopic evidence for interfacial Fe(II)-Fe(III) electron transfer in a clay mineral. Environ. Sci. Technol. 45, 540-545.

Scheidegger, A., Borkovec, M., Sticher, H., 1993. Coating of silica sand with goethite: preparation and analytical identification. Geoderma 58, 43–65.

Schwertmann, U., Thalmann, H., 1976. The influence of [Fe(II)], [Si], and pH on the formation of lepidocrocite and ferrihydrite during oxidation of aqueous $FeCl_2$ solutions. Clay Minerals 11, 189-200.

Schwertmann, U., Cornell, R.M., 2000. Iron oxides in the laboratory: preparation and characterization, WILEY-VCH Verlag GMBH & Co. KGaA, Weinheim, Germany.

Shimizu, M., Zhou, J., Schröder, C., Obst, M., Kappler, A., Borch, T., 2013. Dissimilatory reduction and transformation of ferrihydrite-humic acid coprecipitates. Environ. Sci. Technol. 47, 13375–13384.

Six, J., Elliott, E.T., Paustian, K., Doran, J.W., 1998. Aggregation and soil organic matter accumulation in cultivated and native grassland soils. Soil Sci. Soc. Am. J. 62, 1367-1377.

Soil Survey Staff, 2014. Keys to soil taxonomy. Soil Conserv. Serv. 12, 410.

Stumm, W., Sulzberger, B., 1992. The cycling of iron in natural environments: Considerations based on laboratory studies of heterogeneous redox processes. Geochim. Cosmochim. Acta 56, 3233–3257.

Sun, T., Levin, B.D.A., Guzman, J.J.L., Enders, A., Muller, D.A., Angenent, L.T., Lehmann, J., 2017. Rapid electron transfer by the carbon matrix in natural pyrogenic carbon. Nat. Commun. 8, 1–12.

Sun, T., Levin, B.D.A., Schmidt, M.P., Guzman, J.J.L., Enders, A., Martínez, C.E., Muller, D.A., Angenent, L.T., Lehmann, J., 2018. Simultaneous quantification of electron transfer by carbon matrices and functional groups in pyrogenic carbon. Environ. Sci. Technol. 52, 8538–8547.

Tamrat, W.Z., Rose, J., Grauby, O., Doelsch, E., Levard, C., Chaurand, P., Basile-Doelsch, I., 2019. Soil organo-mineral associations formed by co-precipitation of Fe, Si and Al in presence of organic ligands. Geochim. Cosmochim. Acta 260, 15–28.

ThomasArrigo, L.K., Mikutta, C., Byrne, J., Kappler, A., Kretzschmar, R., 2017. Iron(II)-catalyzed iron atom exchange and mineralogical changes in iron-rich organic freshwater flocs: an iron isotope tracer study. Environ. Sci. Technol. 51, 6897–6907.

ThomasArrigo, L.K., Byrne, J. M., Kappler, A., Kretzschmar, R., 2018. Impact of organic matter on iron(II)-catalyzed mineral transformations in ferrihydrite-organic matter coprecipitates. Environ. Sci. Technol. 52, 12316–12326.

ThomasArrigo, L.K., Kaegi, R., Kretzschmar, R., 2019. Ferrihydrite growth and transformation in the presence of ferrous iron and model organic ligands. Environ. Sci. Technol. 53, 13636-13647.

Tomaszewski, E.J., Cronk, S.S., Gorski, C.A., Ginder-Vogel, M., 2016. The role of dissolved Fe(II) concentration in the mineralogical evolution of Fe (hydr)oxides during redox cycling. Chem. Geol. 438, 163–170.

Usman, M., Abdelmoula, M., Hanna, K., Grégoire, B., Faure, P., Ruby, C., 2012. Fe^{II} induced mineralogical transformations of ferric oxyhydroxides into magnetite of variable stoichiometry and morphology. J. Solid State Chem. 194, 328–335.

von Lützow, M., Kögel-Knabner, I., Ekschmitt, K., Matzner, E., Guggenberger, G., Marschner, B., Flessa, H., 2006. Stabilization of organic matter in temperate soils: mechanisms and their relevance under different soil conditions - a review. Eur. J. Soil Sci. 57, 426–445.

Xiao, J., He, X., Hao, J., Zhou, Y., Zheng, L., Ran, W., Shen, Q., Yu, G., 2016. New strategies for submicron characterization the carbon binding of reactive minerals in long-term contrasting fertilized soils: implications for soil carbon storage. Biogeosciences 13, 3607–3618.

Yang, J., Wang, J., Pan, W., Regier, T., Hu, Y., Rumpel, C., Bolan, N., Sparks, D.L., 2016. Retention mechanisms of citric acid in ternary kaolinite-Fe(III)-citrate acid systems using Fe K-edge EXAFS and $L_{3,2}$-edge XANES spectroscopy. Sci. Rep. 6, 1–9.

Yang, L., Steefel, C.I., Marcus, M.A., Bargar, J.R., 2010. Kinetics of Fe(II)-catalyzed transformation of 6-line ferrihydrite under anaerobic flow conditions. Environ. Sci. Technol. 44, 5469–5475.

Yang, Z., Sun, T., Subdiaga, E., Obst, M., Haderlein, S.B., Maisch, M., Kretzschmar, R., Angenent, L.T., Kappler, A., 2020. Aggregation-dependent electron transfer via redox-active biochar particles stimulate microbial ferrihydrite reduction. Sci. Total Environ. 703, 135515.

Yee, N., Shaw, S., Benning, L.G., Nguyen, T.H., 2006. The rate of ferrihydrite transformation to

goethite via the Fe(II) pathway. Am. Mineral. 91, 92–96.

Yuan, Y., Bolan, N., Prévoteau, A., Vithanage, M., Biswas, J.K., Ok, Y.S., Wang, H., 2017. Applications of biochar in redox-mediated reactions. Bioresour. Technol. 246, 271–281.

Zhou, Z., Latta, D.E., Noor, N., Thompson, A., Borch, T., Scherer, M.M., 2018. Fe(II)-catalyzed transformation of organic matter-ferrihydrite coprecipitates: a closer look using Fe isotopes. Environ. Sci. Technol. 52, 11142–11150.

Zhu, Y., Elzinga, E.J., 2014. Formation of layered Fe(II)-hydroxides during Fe(II) sorption onto clay and metal-oxide substrates. Environ. Sci. Technol. 48, 4937-4945.

Zhu, Y., Liu, J.J., Goswami, O., Rouff, A.A., Elzinga, E.J., 2018. Effects of humic substances on Fe(II) sorption onto aluminum oxide and clay. Geochem. Trans, 19.

Beatrice Giannetta: Conceptualization, Methodology, Writing – Original Draft, **Ramona Balint:** Methodology, Investigation, **Daniel Said-Pullicino:** Supervision, Writing – Review & Editing, **César Plaza:** Funding acquisition, Writing – Review & Editing, **Maria Martin**: Methodology, Writing – Review & Editing, **Claudio Zaccone:** Supervision, Writing – Review & Editing.

Figure captions

Figure 1. Fe K-edge spectra of Fe(III) reference materials.

Figure 2. Fe K-edge EXAFS spectra of the final mineral phases from the Fe(II)-catalyzed transformation experiments of the bulk soils unamended (UN), amended with compost (MC), biochar (BC), and compost and biochar (BC+MC) at pH 7. The red dotted lines represent the linear combination fits of the sample spectra (n=3). R-factors for the fits are displayed.

Figure 3. Fe K-edge EXAFS spectra of the final mineral phases from the Fe(II)-catalyzed transformation experiments of the fine sand (FSa) and fine silt plus clay (FSi+Cl) fractions of the unamended soil (UN), and soils amended with compost (MC), biochar (BC), and compost and biochar (BC+MC) at pH 7. The red dotted lines represent the linear combination fits of the sample spectra (n=3). R-factors for the fits are displayed.

Figure 4. Distribution of Fe references in linear combination fits of k^3-weighted Fe EXAFS spectra of the mineral phases in (a) FSa and (b) FSi+Cl fractions of the unamended soil (UN) and soils amended with compost (MC), biochar (BC), and compost and biochar (BC+MC) before (–Fe(II)) and after (+Fe(II)) the Fe(II)-catalyzed transformation.

Figure 1

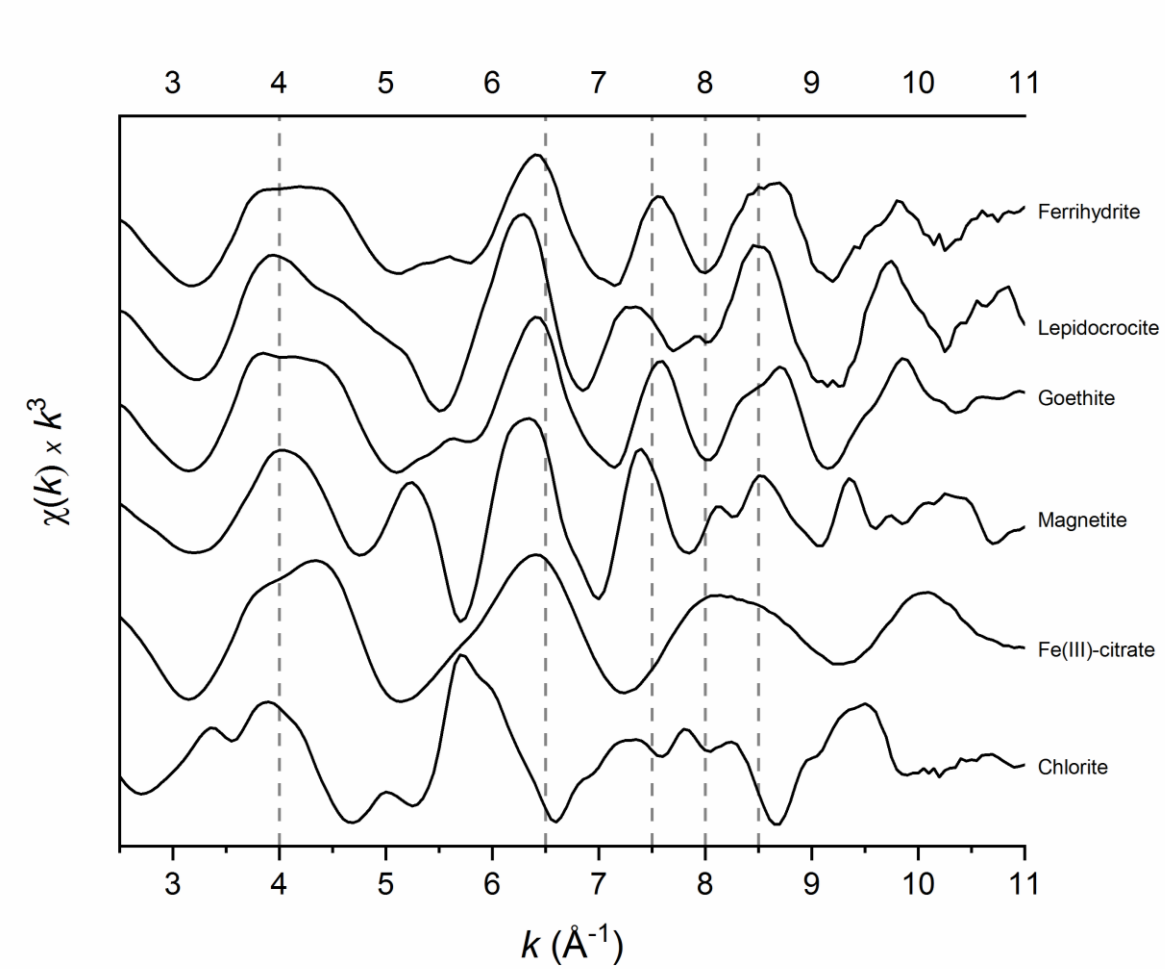
3
4
5
6
7
8
9
10
11
Ferrihydrite
Lepidocrocite
Goethite
Magnetite
Fe(III)-citrate
Chlorite
χ(k) x k3
k (Å-1)

Figure 2

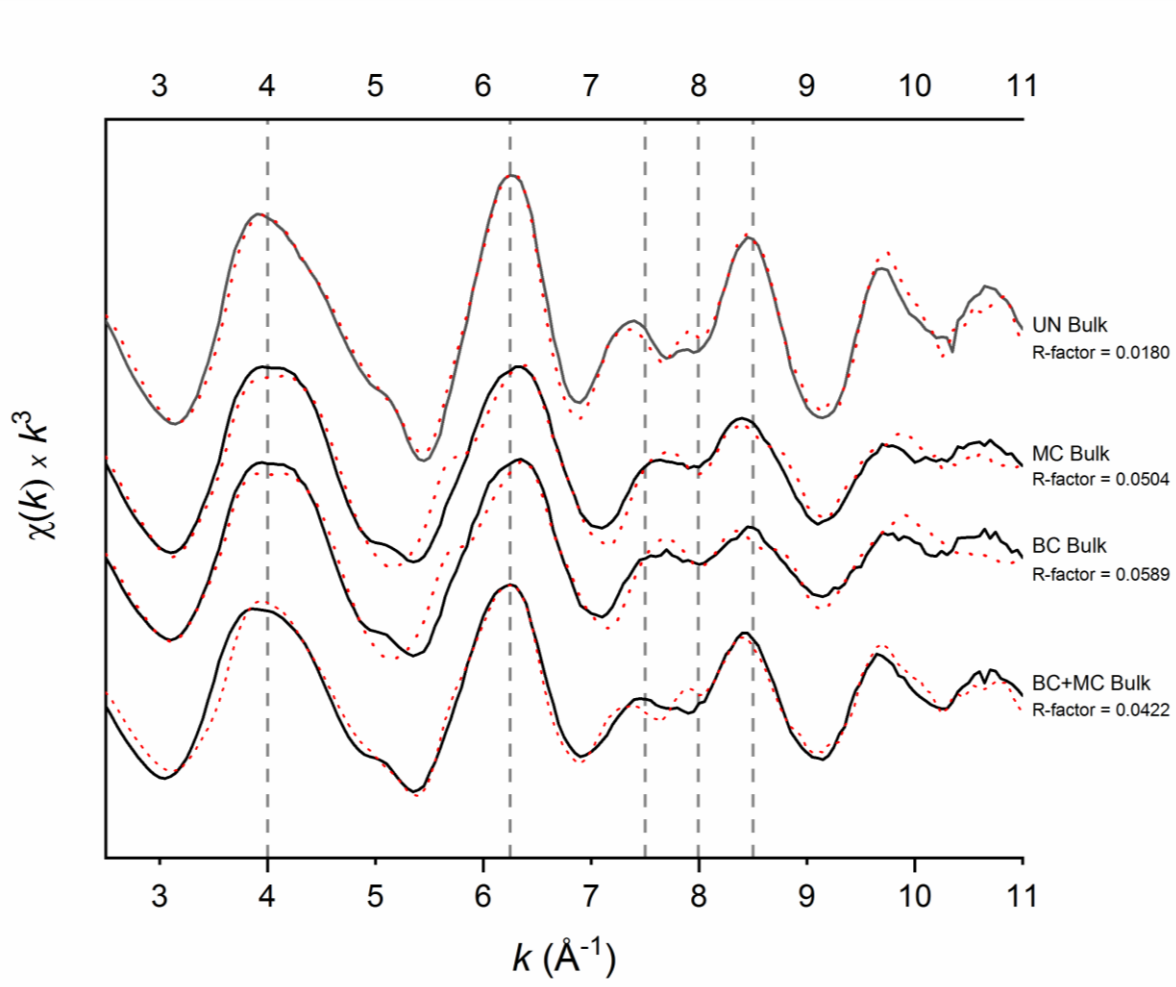
3
4
5
6
7
8
9
10
11
χ(k) x k3
k (Å-1)
UN Bulk
R-factor = 0.0180
MC Bulk
R-factor = 0.0504
BC Bulk
R-factor = 0.0589
BC+MC Bulk
R-factor = 0.0422

Figure 3

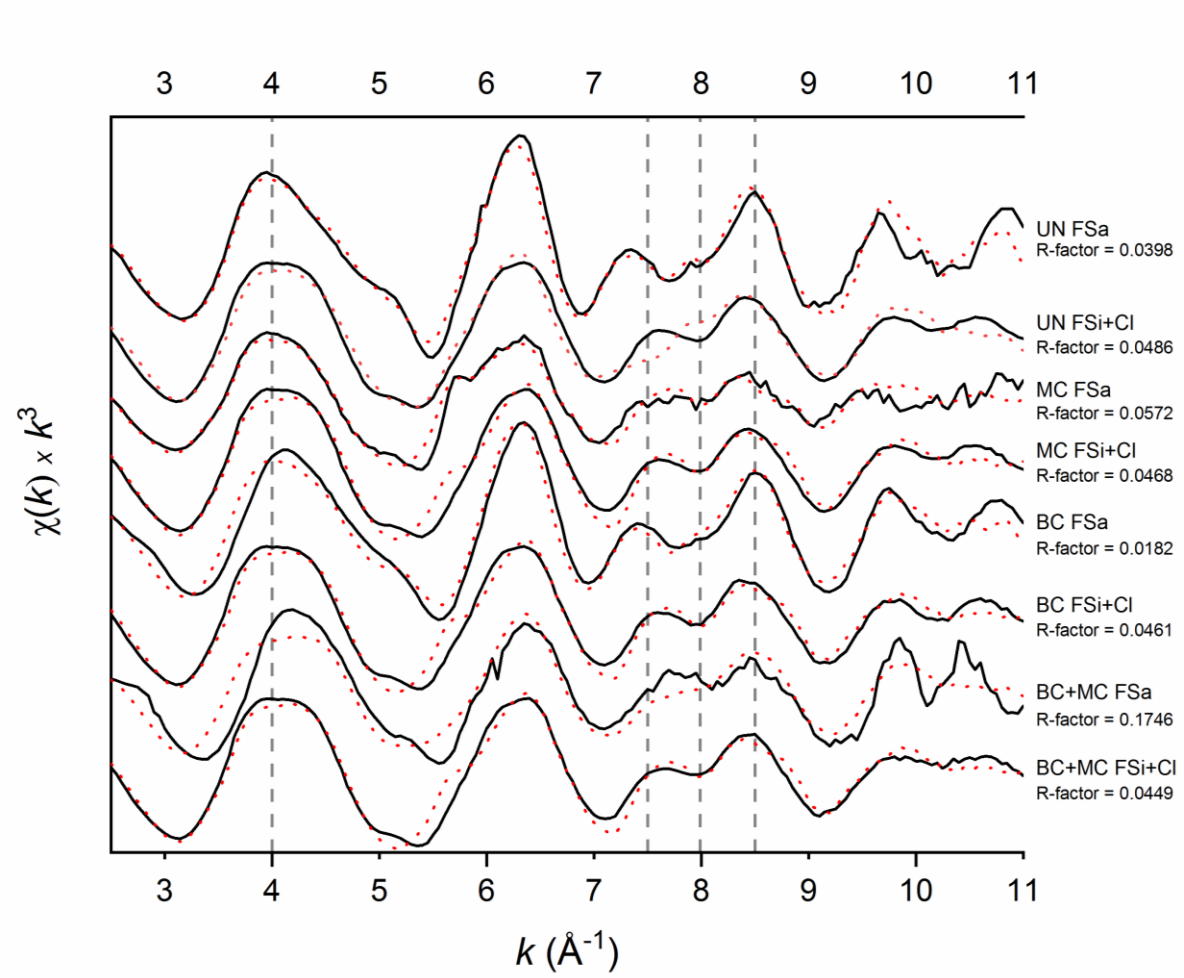
3
4
5
6
7
8
9
10
11
χ(k) x k3
k (Å-1)
UN FSa
R-factor = 0.0398
UN FSi+Cl
R-factor = 0.0486
MC FSa
R-factor = 0.0572
MC FSi+Cl
R-factor = 0.0468
BC FSa
R-factor = 0.0182
BC FSi+Cl
R-factor = 0.0461
BC+MC FSa
R-factor = 0.1746
BC+MC FSi+Cl
R-factor = 0.0449

Figure 4

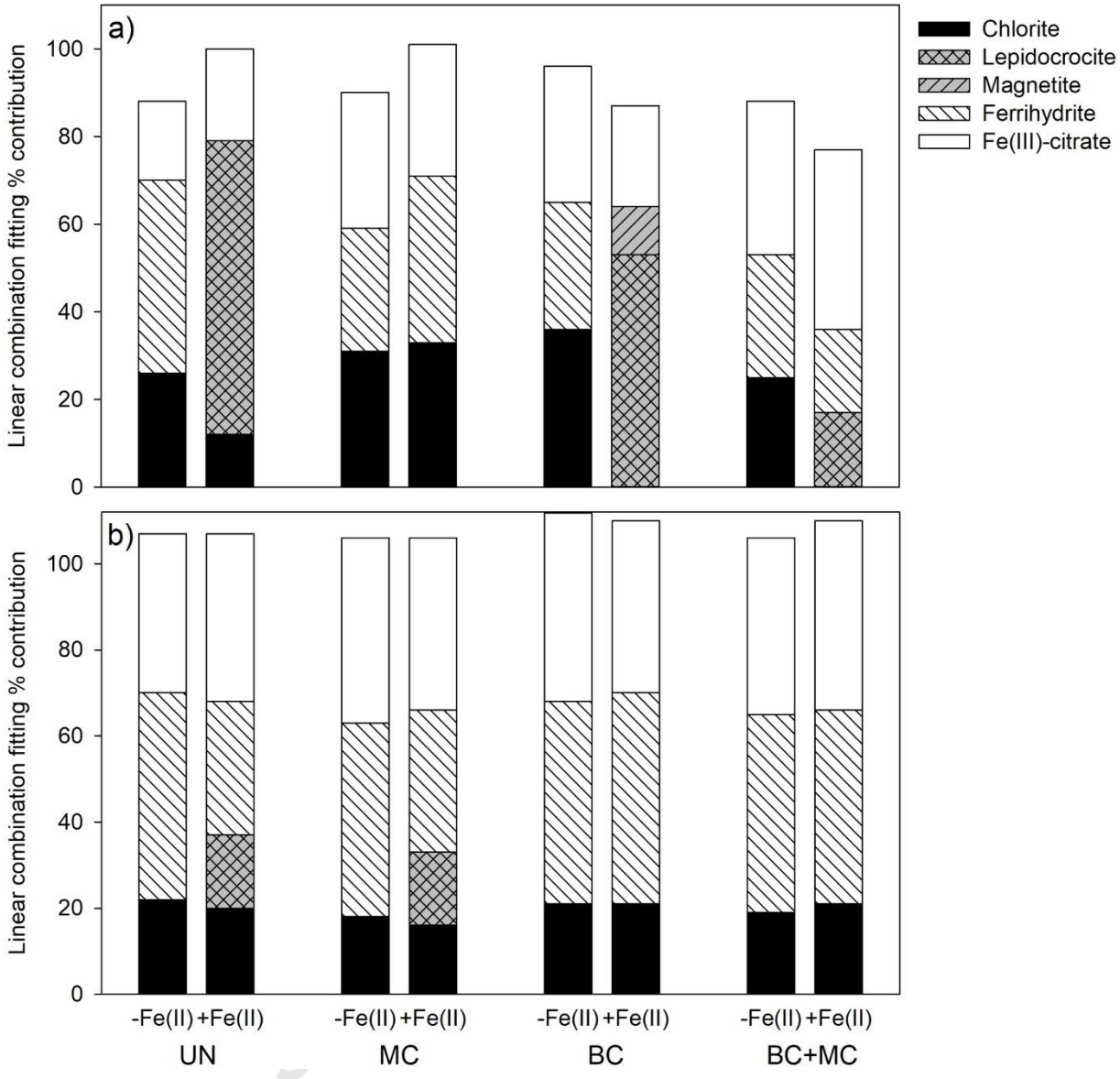
a)
b)
Linear combination fitting % contribution
0
20
40
60
80
100
Chlorite
Lepidocrocite
Magnetite
Ferrihydrite
Fe(III)-citrate
-Fe(II) +Fe(II)
UN
MC
BC
BC+MC

Table 1. Total organic C content, total N, C/N ratio (mean ± standard error) of the agricultural soil unamended (UN) or amended with biochar (BC), municipal solid waste compost (MC) or both (BC+MC). Data from Plaza et al. (2016) and Giannetta et al. (2020a).

Soil	**Total organic C** *($g \cdot kg^{-1}$)*	**Total N** *($g \cdot kg^{-1}$)*	**C/N**	**Fe** *($g \cdot kg^{-1}$)*
UN	11.8±0.7	1.10±0.05	10.7±0.6	22.1±0.3
MC	14.2±0.7	1.31±0.05	10.8±0.6	21.9±1.0
BC	19.8±0.7	1.08±0.05	18.6±0.6	22.1±0.6
BC+MC	22.6±0.7	1.42±0.05	15.9±0.6	22.7±0.5

Table 2. Organic C, total N (data from Giannetta et al. 2020a), mass fractions, and Fe contents of the fine sand (FSa) and fine silt and clay (FSi+Cl) size-fractions of unamended soils (UN) and soils amended with municipal solid waste compost (MC), biochar (BC) or both (BC+MC).

	FSa				**FSi+Cl**	
	Mass fraction *(%)*	**Organic C** *(g kg^{-1})*	**Total N** *(g kg^{-1})*	**Fe** *(g kg^{-1})*	**Mass fraction** *(%)*	**Organic C** *(g kg^{-1})*
UN	27	3.5	0.26	7.9	39	18.1
MC	26	4.6	0.37	8.8	40	20.8
BC	27	8.2	0.33	7.8	37	25.1
BC+MC	26	9.1	0.41	9.8	39	28.2

Declaration of interests

☒ The authors declare that they have no known competing financial interests or personal relationships that could have appeared to influence the work reported in this paper.

☐The authors declare the following financial interests/personal relationships which may be considered as potential competing interests:

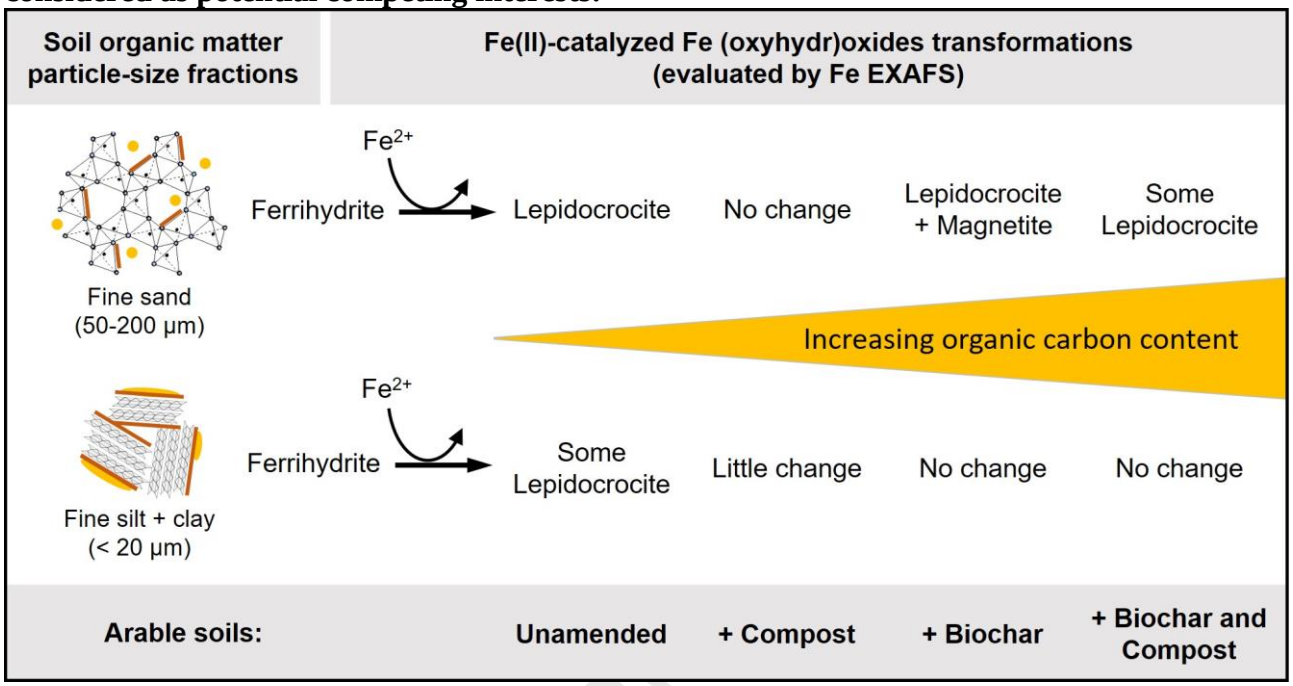

Graphical abstract

Highlights: •

SOM in different pools affects Fe(III) oxides transformation under reducing conditions. • Organic amendments limit abiotic Fe(II)-catalyzed ferrihydrite transformation. • Fe oxide transformation is less evident in fine vs coarse fractions. • In the coarse fraction, Fe(II) addition lead to the transformation of ferrihydrite. • Biochar addition favors the formation of lepidocrocite and magnetite.